Fabrication of Patterned Polymer Nanowire Arrays

Hao Fang,[†,‡] Dajun Yuan,[§] Rui Guo,[§] Su Zhang,[‡] Ray P. S. Han,[†] Suman Das,[§] and Zhong Lin Wang[‡,*]

[†]Department of Advanced Materials and Nanotechnology, College of Engineering, Peking University, Beijing 100871, People's Republic of China, [‡]School of Materials Science and Engineering, Georgia Institute of Technology, Atlanta, Georgia 30332, USA, and [§]Woodruff School of Mechanical Engineering, Georgia Institute of Technology, Atlanta, Georgia 30332, USA

ABSTRACT A method for the large-scale fabrication of patterned organic nanowire (NW) arrays is demonstrated by the use of laser interference patterning (LIP) in conjunction with inductively coupled plasma (ICP) etching. The NW arrays can be fabricated after a short ICP etching of periodic patterns produced through LIP. Arrays of NWs have been fabricated in UV-absorbent polymers, such as PET (polyethylene terephthalate) and Dura film (76% polyethylene and 24% polycarbonate), through laser interference photon ablation and in UV transparent polymers such as PVA (polyvinyl acetate) and PP (polypropylene) through laser interference lithography of a thin layer of photoresist coated atop the polymer surface. The dependence of the structure and morphology of NWs as a function of initial pattern created by LIP and the laser energy dose in LIP is discussed. The absence of residual photoresist atop the NWs in UV-transparent polymers is confirmed through Raman spectroscopy.

KEYWORDS: organic nanowire arrays · laser interference patterning

One-dimensional nanomaterial devices of inorganic semiconductors and functional oxides have been studied for application in electrics, mechanics, photonics, bioscience, and energy science.[1−9] Fabrication of patterned inorganic nanowires (NW) has been widely developed *via* different methods, such as electron beam lithography (EBL),[10] nanoimprint lithography (NIL),[11,12] and nanosphere lithography (NSL).[13−15] Polymer-based NWs have been fabricated and demonstrated for applications in areas such as organic light-emitting diodes (OLED), field-effect transistors (FET), sensors, and organic solar cells.[16−19] Demonstrated approaches for the fabrication of organic NWs include EBL, electrochemical deposition, and anodic aluminum oxide (AAO).[20−22] However none of these approaches provide a reliable, high-throughput, and low-cost solution for large-scale fabrication of patterned organic NW arrays at a level required for industrial applications.

We have previously demonstrated a fabrication method using a single-step inductively coupled plasma (ICP) etching to get wafer-scale aligned NW arrays from commercial polymer films and functional organic materials, such as PMMA (poly(methyl methacrylate)), PS (polystyrene), PDMS (polydimethylsiloxane), PET (polyethylene terephthalate), PEDOT/PSS (poly(3,4-ethylenedioxythiophene)poly(styrenesulfonate)), and MEH-PPV (poly[2-methoxy-5-(2-ethylhexyloxy)-1,4-phenylenevinylene]).[23] The density and length of NWs can be easily controlled *via* different thicknesses of deposited gold and the etching time.[24] However an ordered, period controllable NW array is still needed for further applications of functional devices such as OLEDs, OFETs, and solar cells.[25−27]

Laser interference patterning (LIP) is known as a reliable and fast technique to achieve large-area periodic patterns and can be used to form an initial pattern on polymer films.[28−30] In this paper, we combine the pattern generating technology by LIP and ICP etching to fabricate ordered and large-scale polymer NW arrays with high-throughput on both UV-absorbent polymers including PET and Dura film (76% PE (polyethylene) (76%) and polycarbonate (24%)) and UV-transparent polymers such as PVA (polyvinyl acetate) and PP (polypropylene). The NW arrays can be fabricated after a short ICP etching of periodic patterns produced through LIP.

RESULTS AND DISCUSSION

Details about the LIP technique have been introduced previously.[29,30] Briefly, the interference period (P_d) is determined by the wavelength (λ) and the angle (θ) and is given by $P_d = \lambda/2 \sin(\theta/2)$. In the LIP experiments described here, the laser wavelength is 266 nm. By changing the angle between two laser beams, the period can be easily changed from approximately $\lambda/2$ to several hundreds of micrometers. The exposure dose is another important experimental parameter. By increasing the exposure dose, both the width and the depth of the

*Address correspondence to zlwang@gatech.edu.

Received for review December 5, 2010 and accepted December 22, 2010.

Published online December 31, 2010
10.1021/nn103319p

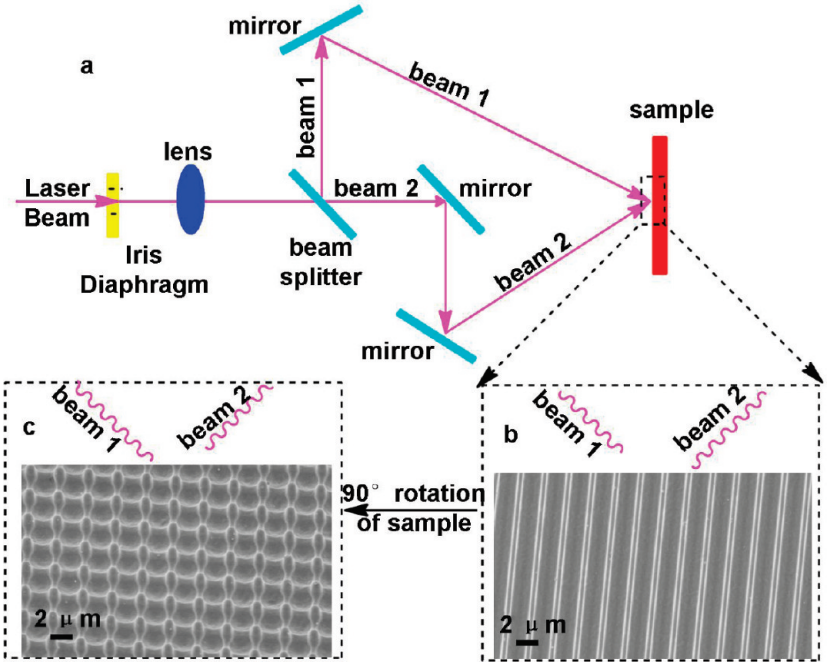

Figure 1. Schematic of the experimental setup for laser interference patterning (LIP). (a) The 266 nm wavelength was split into two coherent beams (beam 1 and beam 2) with pulses lasting 10 ns and repetition of 10 Hz. (b) Interference of beam 1 and beam 2 formed a grating pattern on Dura film (SEM image, 2.5 μm period). (c) Nanodots pattern was formed by the LIP after a 90° rotation of the Dura film (SEM image, 2.5 μm period).

ablation trench increase, which follows the widely accepted form of Beer's law:

$$d(F) = \frac{1}{\alpha_{\text{eff}}} \ln\left(\frac{F}{F_{\text{th}}}\right)$$

It represents the ablation depth (d) at various exposure dose (F), the threshold exposure dose (F_{th}), and the effective absorption coefficient (α_{eff}).[31]

A commercial Nd:YAG laser (Quanta-Ray PRO 290, Spectra Physics) was utilized in the laser interference patterning experiments. The fundamental wavelength of the Nd:YAG laser is 1064 nm, from which shorter wavelengths (532, 355, and 266 nm) can be obtained by harmonic generation. The third-harmonic wavelength of 266 nm was used to irradiate the samples with pulses lasting 10 ns at a repetition rate of 10 Hz.

The P-polarized laser beam was split into two beams by a 50/50 beam splitter and then recombined at the sample surface with a designated interference angle (θ). The interference period (P_d) is determined by the wavelength (λ) and the angle (θ) and is given by the equation $P_d = \lambda/2 \sin(\theta/2)$. The laser power could be adjusted through the laser controller and was monitored by a high damage threshold power meter together with a 10% reflection beam splitter. The exposure time was controlled by a mechanical shutter (Uniblitz Electronic VS25S2ZMO) with a temporal resolution of 3.0 ms. Samples were loaded on a manually actuated precision rotation stage and exposed to the pulsed interference pattern. All of the experiments were performed in an ambient atmosphere environment (Figure 1).

For direct laser interference patterning of UV-absorbent polymers, the precleaned polymers were loaded on the rotation stage. Exposure to the periodic intensity distribution of the interference patterns leads to selective and periodic photon ablation of the sample surface. Successive exposures with a rotation of 90° between exposures create a crossed-grid pattern of photon-ablated lines in the regions of high intensity and an array of spherical convex shapes in the regions of low intensity (Figure 2a). For UV-transparent polymers, a thin film of photoresist was spin-coated on the surface to form the initial pattern for further ICP etching (Figure 2b). Hexagonal patterns could also be produced by simply rotating the sample by 60° twice between successive LIP patterning shots (Figure 3a).

After the LIP of either UV-absorbent or -transparent polymers, the patterned polymer films were placed in an ICP etching chamber for a one-step plasma reactive ion etching process, which has been introduced previously.[23,24] The gases Ar, O_2, and CF_4 were introduced into the ICP chamber with flow ratios of 15.0, 10.0, and 30.0 sccm (standard cubic centimeters per minute), respectively. The operating temperature was 55.0 °C with a pressure of 15 mTorr. One power source of 400 W was used to generate a large density of plasma, while another power source of 100 W was used to accelerate plasma ions toward the polymer surface. The processing time could be varied from 1 min to over 1 h. The mechanism of the

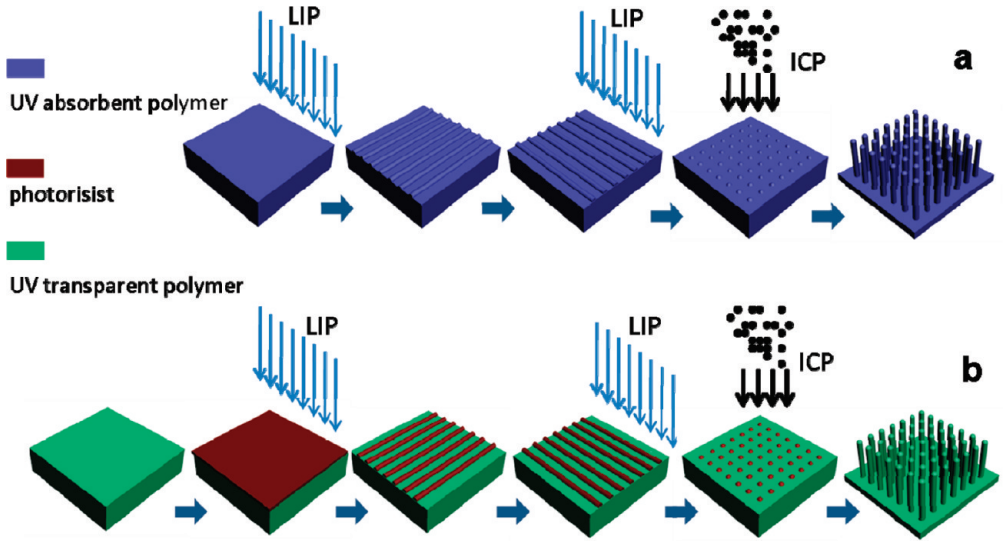

Figure 2. Fabrication processes for UV absorbent and transparent polymers. In (a), LIP was directly applied on UV-absorbent polymers to form the initial patterns, while in (b), a photoresist (PR) was coated on the UV-transparent polymers to produce patterns by LIP for further ICP etching.

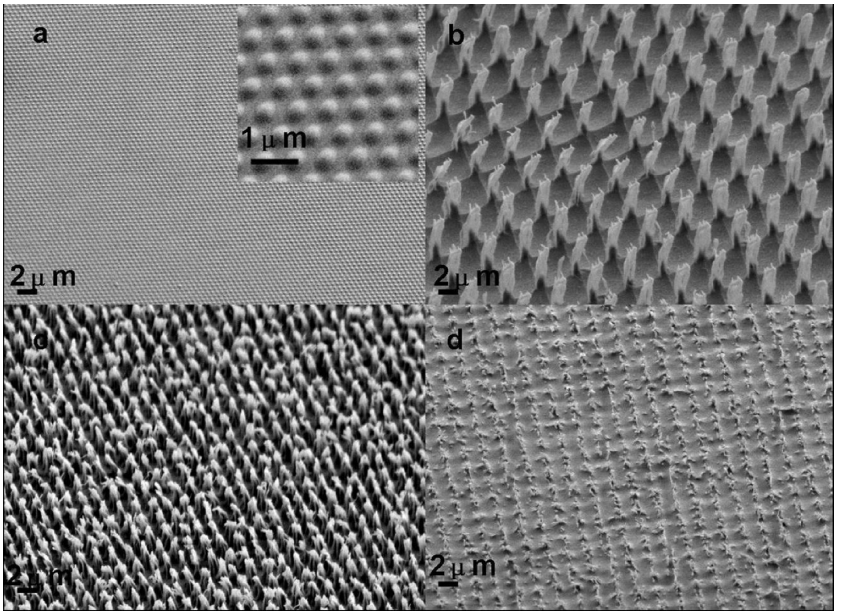

Figure 3. (a) 1 μm period of LIP patterned photoresist 1813 coated on PDMS; (b) 2.5 μm period of PET nanowire array; (c) 2.5 μm period of acetate film nanowire array; (d) 2.5 μm period of PP nanowire array. Inset is enlarged view of 1813 patterned on PDMS.

ICP etching for fabricating NWs has been described previously.[23,24]

Figure 3 shows the SEM images for UV-absorbent polymer (PET, Figure 3b) nanowire array and UV-transparent polymer (acetate film, Figure 3c, and PP, Figure 3d) nanowire arrays. The period of these PNWs arrays is 2.5 μm, while the morphology of the PNWs is nearly the same after the ICP etching.

The chemical structures of polymers determined if the polymers can be directly used for the LIP to form a pattern or need an additional step to make an initial pattern. Figure 4 shows several chemical structures of different polymers that have been used in our study. PS, PET, and polycarbonate are visible light transparent polymer materials, while they have good absorption of UV wavelengths, so these materials can be used directly in the LIP process. The phenyl group in these polymer structures gives the polymers good absorption of UV wavelengths, while the other UV-transparent polymers such as PE, PP, and polyvinyl acetate have only single C−C bonds, which do not have strong absorption in the UV wavelength range. The composition of the Dura film is a mixture of PE (76%) and polycarbonate (24%). With 24% polycarbonate, the

Dura film has good absorption of UV wavelengths. Since we cannot produce patterns directly on UV-transparent polymers using LIP, a UV-absorbent layer is required on these polymers to produce the initial pattern. Photoresists are UV-absorbent materials widely used for pattern generation in photolithography (using UV lamps or UV wavelength lasers) for the fabrication of micrometer and submicrometer scale structures. Photoresists can be applied as thin films underlying polymer films to create a highly UV absorbent layer for subsequent LIP.

The morphology of the PNWs arrays are determined by the initial pattern and the etching time. Figure 5a shows a 1 μm period pattern on Dura film, which forms a 1 μm period PNWs array after ICP etching for several minutes. The periods can be controlled from 200 nm to several micrometers. Figure 5b–d shows the patterns generated by controlling the periodicity from 2.5 μm to 500 nm. The diameters of the PNWs are different for different periods of the PNWs arrays. The diameter increases with increasing period, which is around 100 nm in the 500 nm period PNWs array and up to 500 nm in the 2.5 μm period array. The difference in the diameters of the PNWs can be explained through a growth mechanism described in previous literature. The initial pattern's diameter determines the diameter of the PNWs, which changes negligibly during the ICP etching process. The etching process has a large etching ratio on the bottom of the polymer surface, while the etching ratio is quite small at the top and the side walls of the PNWs. Thus, the diameter of PNWs is primarily determined by the patterns created through LIP.

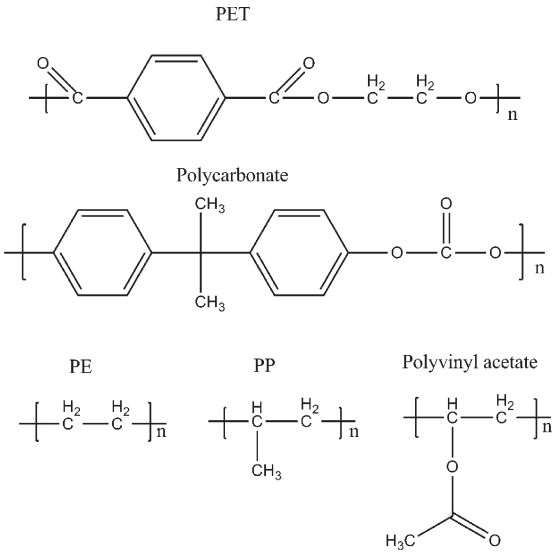

Figure 4. Chemical structures of UV-absorbent polymers (PET, polycarbonate) and UV-transparent polymers (PE, PP, and PVA).

The energy dose in LIP has a significant effect on the morphology of the patterned PNWs array. Figure 6 shows the different morphologies of Dura films before and after the ICP etching using different energy doses during the LIP process. The depths of the photon-ablated patterned trenches become deeper and more well-defined with increasing energy dose, as expected. However, the energy dose should be limited so as to create only the initial patterns on the polymer film surface and to prevent ablation through the entire film thickness (see Figure 6a–c), which would perforate the film and prevent further development of nanostructures. Once the initial nanoscale patterns are created by LIP, ICP etching can be utilized to produce longer PNWs. Both the patterns and the morphologies of subsequently produced PNWs change as a function

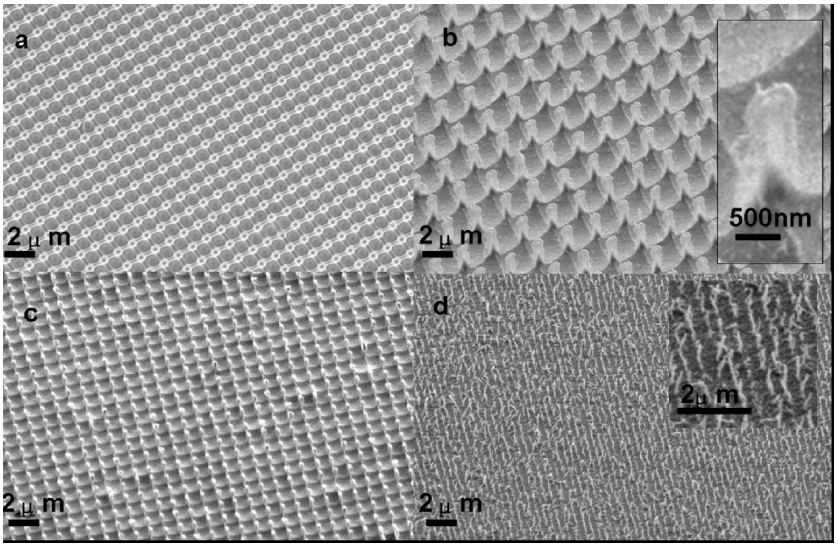

Figure 5. Different periods of patterned PNWs arrays on Dura film: (a) 1 μm period of LIP pattern on Dura film; (b) 2.5 μm period of Dura nanowire array; (c) 1 μm period of Dura nanowire array; (d) 500 nm period of Dura nanowire array. Insets are the enlarged view of a single NW in a 2.5 μm period of Dura nanowire array and the enlarged view of NWs in a 500 nm period of Dura nanowire array.

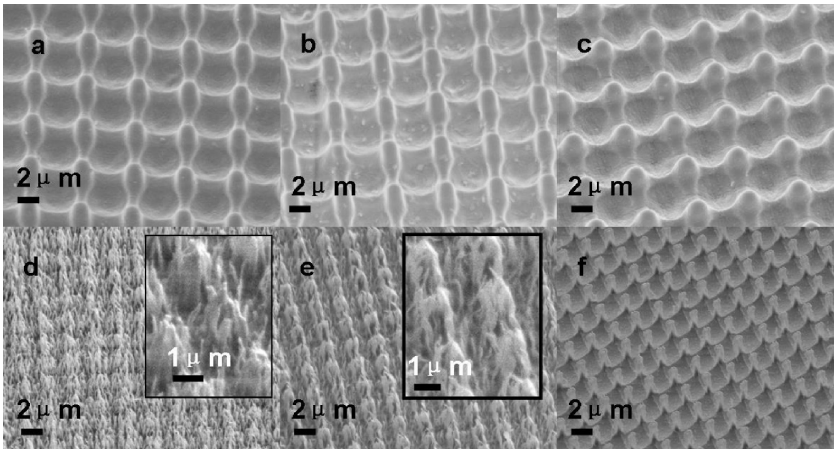

Figure 6. Effect on patterns and NWs arrays of Dura film with different laser powers: (a, b, c) 2.5 μm period of patterns on Dura film with laser power of 40, 90, and 110 mJ/cm^2, respectively; (d, e, f) 2.5 μm period of PNWs on Dura film with laser power of 40, 90, and 110 mJ/cm^2, respectively. Insets are the enlarged view of PNWs in each picture, respectively.

of the energy dose in LIP. Figure 6d, e, and f shows the morphology of the PNWs array after etching of patterns created with a low-energy dose in LIP. Only clusters of small PNWs (Figure 6d) rather than individual PNWs can be produced in this case. The clusters become smaller with increasing energy dose (Figure 6e). At still higher energy dose, the clusters of small PNWs are absent and well-formed individual PNWs begin to form (Figure 6f). This phenomenon also can be explained from the growth mechanism of the PNWs. When the energy dose in LIP is low, the edge of each patterned nanodot is not very well-defined, which makes the formation a well-defined side wall of each PNW difficult in subsequent ICP etching. In this case, only clusters of small PNWs can be formed after the ICP etching process. However, with increasing energy dose, the edge and the sidewall of the nanodots are well-defined and the ablated trench is deeper, which makes the cluster smaller and the PNWs bigger. At still higher energy doses, the edge and sidewall of each nanodot are distinct and very well-defined, leading to the formation of an array of periodically placed individual PNWs.

After the ICP etching, the chemical structure remains unchanged according to previous literature reports.[24] For the UV-absorbent polymers, LIP only ablated the polymer surface and the ICP etching cannot change the chemical properties of the polymer. The UV-transparent polymers, however, have an initial photoresist pattern layer on the surface before ICP etching. Raman spectroscopy was used to determine if the photoresist was still present on the top of the PNWs after etching. Figure 7 shows the Raman spectrum of the PDMS surface during the different process steps. Figure 7, curve e, shows there are two wide peaks at 3000−4000 and 1000−2000 cm^{-1} for the photoresist 1813. After we spin-coated the photoresist on the PDMS film surface at the speed of 4000 rpm for 45 s and baked for 90 s, the Raman spectrum of the photoresist-coated PDMS (Figure 7, curve d) has two wide peaks at 3000−4000 and 1000−2000 cm^{-1}, which are the same as for pure photoresist 1813. Furthermore, there are two small sharp peaks around 2966 and 2906 cm^{-1}, which are the same as for the spectrum of the pure PDMS (Figure 7, curve a). However, the densities of the two peaks are quite small compared to the peaks of photoresist 1813. The whole surface of the PDMS surface is coated with photoresist and the detection depth of the Raman spectrum is not sufficiently deep enough to obtain high signals of the PDMS under the photoresist 1813 layer. However, after the initial pattern made by LIP on the 1813-coated PDMS, the densities of the two sharp peaks around 2966 and 2906 cm^{-1} (Figure 7, curve c) increased considerably as compared to the densities of the two wide peaks from the photoresist 1813. The change in the density of PDMS and 1813 shows that the PDMS has been exposed at its surface and most of the photoresist 1813 has been vaporized after the LIP. Only the initial 1813 pattern existed on the PDMS surface (Figure 3a). After the ICP etching for several minutes, the spectrum of the PNWs array (Figure7, curve b) is the same as the spectrum of the pure PDMS (Figure 7, curve a), which means that the chemical structure of the PMDS PNWs array did not change after the ICP etching. The initial 1813 pattern might have been etched out during the process, as the thickness of the 1813 is quite small and the etching process still has a little etching ratio for the 1813 pattern on the tops of the PNWs on the PDMS surface.

In summary, we have combined the laser interference patterning technique and inductively coupled plasma etching for the fabrication of ordered polymer nanowire arrays in both UV-absorbent and UV-transparent polymers. The period of the pattern can be easily controlled and varied from 500 nm to several micrometers using LIP. The energy dose used for the initial patterning has a significant impact on the

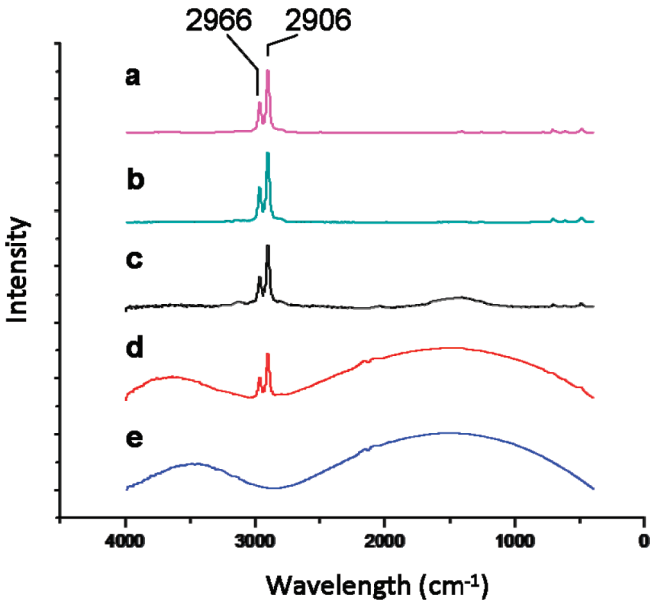

Figure 7. Raman spectra of PR 1813 and PDMS: (a) spectrum of pure PDMS with two sharp peaks around 2966 and 2906 cm^{-1}; (b) spectrum of PDMS NWs array with two sharp peaks around 2966 and 2906 cm^{-1}; (c) spectrum of PDMS with PR 1813 pattern with two high sharp peaks around 2966 and 2906 cm^{-1} and a wide peak between 1000 and 2000 cm^{-1}; (d) spectrum of PR 1813 spin-coated on PDMS with two small sharp peaks around 2966 and 2906 cm^{-1} and two wide peaks at 3000−4000 and 1000−2000 cm^{-1}; (e) spectrum of pure PR 1813 with two wide peaks at 3000−4000 and 1000−2000 cm^{-1}.

morphology of the PNWs array. The photoresist will not remain on the top of the PDMS PNWs according to the Raman spectrum result. This method demonstrates an efficiency approach to fabricate organic material devices in mechanic, electrical, energy, and biological science.

EXPERIMENTAL SECTION

A commercial Nd:YAG laser (Quanta-Ray PRO 290, Spectra Physics) was utilized in the laser interference patterning experiments. The laser power was adjusted through the laser controller and was monitored by a high damage threshold power meter together with a 10% reflection beam splitter. The exposure time was controlled by a mechanical shutter (Uniblitz Electronic VS25S2ZMO) with a temporal resolution of 3.0 ms. Samples were loaded on a manually actuated precision rotation stage and exposed to the pulsed interference pattern. All the experiments were performed in an ambient atmosphere environment. LIP was directly applied on precleaned UV-transparent polymers to form a grating pattern. After the 90° rotation of the sample manually, LIP was applied on the sample again to make the nanodots array for further ICP etching. The only difference in the process for UV-transparent polymers was that a thin film of photoresist was spin-coated on the polymer film before LIP. The gases Ar, O_2, and CF_4 were introduced in the ICP chamber with flow ratios of 15.0, 10.0, and 30.0 sccm, respectively. The operating temperature was 55.0 °C with a pressure of 15 mTorr. One power source of 400 W was used to generate a large density of plasma, while another power source of 100 W was used to accelerate plasma ions toward the polymer surface. The processing time could be varied from 1 min to over 1 h. A Thermo Nicolet Almega Micro-Raman microscope was used for the Raman spectrum measurement.

Acknowledgment. This research was supported by NSF, BES DOE, the Air Force, and Georgia Institute of Technology. H.F. was a visiting student at the Georgia Institute of Technology and was partially supported by the Chinese Scholars Council.

REFERENCES AND NOTES

1. Iijima, S. Helical Microtubules of Graphitic Carbon. *Nature* **1991,** *354*, 56–58.
2. Cui, Y.; Lieber, C. M. Functional Nanoscale Electronic Devices Assembled Using Silicon Nanowire Building Blocks. *Science* **2001,** *291*, 851–853.
3. Patolsky, F.; Timko, B. P.; Yu, G. H.; Fang, Y.; Greytak, A. B.; Zheng, G. F.; Lieber, C. M. Detection, Stimulation, and Inhibition of Neuronal Signals with High-density Nanowire Transistor Arrays. *Science* **2006,** *313*, 1100–1104.
4. Pauzauskie, P. J.; Yang, P. Nanowire Photonics. *Mater Today* **2006,** *9*, 36–45.
5. Pan, Z. W.; Dai, Z. R.; Wang, Z. L. Nanobelts of Semiconducting Oxides. *Science* **2001,** *291*, 1947–1949.
6. Wang, Z. L. ZnO Nanowire and Nanobelt Platform for Nanotechnology. *Mater. Sci. Eng. Rep.* **2009,** *64*, 33–71.
7. Liu, C. H.; Zapien, J. A.; Yao, Y.; Meng, X. M.; Lee, C. S.; Fan, S. S.; Lifshitz, Y.; Lee, S. T. High-density, Ordered Ultraviolet Light-emitting ZnO Nanowire Arrays. *Adv. Mater.* **2003,** *15*, 838–841.
8. Cui, J. B.; Daghlian, C. P.; Gibson, U. J.; Pusche, R.; Geithner, P.; Ley, L. Low-temperature Growth and Field Emission of ZnO Nanowire Arrays. *J. Appl. Phys.* **2005,** *97*, 044315.
9. Saito, N.; Haneda, H.; Sekiguchi, T.; Ohashi, N.; Sakaguchi, I.; Koumoto, K. Low-temperature Fabrication of Light-emitting Zinc Oxide Micropatterns Using Self-assembled Monolayers. *Adv. Mater.* **2002,** *14*, 418–421.
10. Xu, S.; Wei, Y.; Kirkham, M.; Liu, J.; Mai, W.; Davidovic, D.; Snyder, R. L.; Wang, Z. L. Patterned Growth of Vertically Aligned ZnO Nanowire Arrays on Inorganic Substrates at Low Temperature without Catalyst. *J. Am. Chem. Soc.* **2008,** *130*, 14958–14959.

11. Hochbaum, A. I.; Fan, R.; He, R. R.; Yang, P. D. Controlled Growth of Si Nanowire Arrays for Device Integration. *Nano Lett.* **2005,** *5*, 457–460.
12. Martensson, T.; Carlberg, P.; Borgstrom, M.; Montelius, L.; Seifert, W.; Samuelson, L. Nanowire Arrays Defined by Nanoimprint Lithography. *Nano Lett.* **2004,** *4*, 699–702.
13. Wang, X. D.; Summers, C. J.; Wang, Z. L. Large-scale Hexagonal-patterned Growth of Aligned ZnO Nanorods for Nano-optoelectronics and Nanosensor Arrays. *Nano Lett.* **2004,** *4*, 423–426.
14. Rybczynski, J.; Banerjee, D.; Kosiorek, A.; Giersig, M.; Ren, Z. F. Formation of Super Arrays of Periodic Nanoparticles and Aligned ZnO Nanorods—Simulation and Experiments. *Nano Lett.* **2004,** *4*, 2037–2040.
15. Fan, H. J.; Fuhrmann, B.; Scholz, R.; Syrowatka, F.; Dadgar, A.; Krost, A.; Zacharias, M. Well-ordered ZnO Nanowire Arrays on GaN Substrate Fabricated *via* Nanosphere Lithography. *J. Cryst. Growth* **2006,** *287*, 34–38.
16. Wanekaya, A. K.; Lei, Y.; Bekyarova, E.; Chen, W.; Haddon, R.; Mulchandani, A.; Myung, N. V. Fabrication and Properties of Conducting Polypyrrole/SWNT-PABS Composite Films and Nanotubes. *Electroanalysis* **2006,** *18*, 1047–1054.
17. Thurn-Albrecht, T.; Schotter, J.; Kastle, C. A.; Emley, N.; Shibauchi, T.; Krusin-Elbaum, L.; Guarini, K.; Black, C. T.; Tuominen, M. T.; Russell, T. P. Ultrahigh-density Nanowire Arrays Grown in Self-assembled Diblock Copolymer Templates. *Science* **2000,** *290*, 2126–2129.
18. Chen, Y. X.; Luo, Y. Precisely Defined Heterogeneous Conducting Polymer Nanowire Arrays—Fabrication and Chemical Sensing Applications. *Adv. Mater.* **2009,** *21*, 2040–2044.
19. Cheng, K. H.; Zhong, Y. C.; Xie, B. Y.; Dong, Y. Q.; Hong, Y. N.; Sun, J. Z.; Tang, B. Z.; Wong, K. S. Fabrication of and Ultraviolet Lasing in TPE/PMMA Polymer Nanowires. *J. Phys. Chem. C* **2008,** *112*, 17507–17511.
20. Lee, H.; Lee, B. P.; Messersmith, P. B. A Reversible Wet/Dry Adhesive Inspired by Mussels and Geckos. *Nature* **2007,** *448*, 338–341.
21. Geim, A. K.; Dubonos, S. V.; Grigorieva, I. V.; Novoselov, K. S.; Zhukov, A. A.; Shapoval, S. Y. Microfabricated Adhesive Mimicking Gecko Foot-hair. *Nat. Mater.* **2003,** *2*, 461–463.
22. Liu, J.; Lin, Y. H.; Liang, L.; Voigt, J. A.; Huber, D. L.; Tian, Z. R.; Coker, E.; Mckenzie, B.; Mcdermott, M. J. Templateless Assembly of Molecularly Aligned Conductive Polymer Nanowires: A New Approach for Oriented Nanostructures. *Chem.—Eur. J.* **2003,** *9*, 605–611.
23. Morber, J. R.; Wang, X. D.; Liu, J.; Snyder, R. L.; Wang, Z. L. Wafer-Level Patterned and Aligned Polymer Nanowire/Micro- and Nanotube Arrays on any Substrate. *Adv. Mater.* **2009,** *21*, 2072–2076.
24. Fang, H.; Wu, W. Z.; Song, J. H.; Wang, Z. L. Controlled Growth of Aligned Polymer Nanowires. *J. Phys. Chem. C* **2009,** *113*, 16571–16574.
25. Park, D. H.; Hong, Y. K.; Cho, E. H.; Kim, M. S.; Kim, D. C.; Bang, J.; Kim, J.; Joo, J. Light-Emitting Color Barcode Nanowires Using Polymers: Nanoscale Optical Characteristics. *ACS Nano* **2010,** *4*, 5155–5162.
26. Xu, J. J.; Wang, K.; Zu, S. Z.; Han, B. H.; Wei, Z. X. Hierarchical Nanocomposites of Polyaniline Nanowire Arrays on Graphene Oxide Sheets with Synergistic Effect for Energy Storage. *ACS Nano* **2010,** *4*, 5019–5026.
27. Jalabert, L.; Bottier, C.; Kumemura, M.; Fujita, H. Nanoscale Surface Engineering of PDMS by Embedding Vertical Nanosheets of Materials. *Microelectron. Eng.* **2010,** *87*, 1431–1434.
28. Chong, T. C.; Hong, M. H.; Shi, L. P. Laser Precision Engineering: From Microfabrication to Nanoprocessing. *Laser Photonics Rev.* **2010,** *4*, 123–143.
29. Wei, Y. G.; Wu, W. Z.; Guo, R.; Yuan, D. J.; Das, S. M.; Wang, Z. L. Wafer-Scale High-Throughput Ordered Growth of Vertically Aligned ZnO Nanowire Arrays. *Nano Lett.* **2010,** *10*, 3414–3419.
30. Yuan, D. J.; Guo., R..; Wei, Y. G.; Wu, W. Z.; Ding, Y.; Wang, Z. L.; Das, S. Heteroepitaxial Patterned Growth of Vertically Aligned and Periodically Distributed ZnO Nanowires on GaN Using Laser Interference Ablation. *Adv. Funct. Mater.* **2010,** *20*, 3484–3489.
31. Chu, C. F.; Lai, F. I.; Chu, J. T.; Yu, C. C.; Lin, C. F.; Kuo, H. C.; Wang, S. C. Study of GaN Light-emitting Diodes Fabricated by Laser Lift-off Technique. *J. Appl. Phys.* **2004,** *95*, 3916–3922.